ACS APPLIED MATERIALS & INTERFACES

www.acsami.org Research Article

Polar Rectification Effect in Electro-Fatigued $SrTiO_3$-Based Junctions

Xueli Xu,◆ Hui Zhang,◆ Zhicheng Zhong,* Ranran Zhang, Lihua Yin, Yuping Sun, Haoliang Huang, Yalin Lu, Yi Lu, Chun Zhou, Zongwei Ma, Lei Shen, Junsong Wang, Jiandong Guo, Jirong Sun,* and Zhigao Sheng*

Cite This: *ACS Appl. Mater. Interfaces* 2020, 12, 31645−31651 Read Online

ACCESS | Metrics & More | Article Recommendations | Supporting Information

ABSTRACT: Rectifying semiconductor junctions are crucial to electronic devices. They convert alternating current into a direct one by allowing unidirectional charge flows. Analogous to the current-flow rectification for itinerary electrons, here, a polar rectification that is based on the localized oxygen vacancies (OVs) in a Ti/fatigued-$SrTiO_3$ (fSTO) Schottky junction is first demonstrated. The fSTO with OVs is produced by an electrodegradation process. The different movabilities of localized OVs and itinerary electrons in the fSTO yield a unidirectional electric polarization at the interface of the junction under the coaction of external and built-in electric fields. Moreover, the fSTO displays a pre-ferroelectric state located between paraelectric and ferroelectric phases. The pre-ferroelectric state has three sub-states and can be easily driven into a ferroelectric state by an external electric field. These observations open up opportunities for potential polar devices and may underpin many useful polar-triggered electronic phenomena.

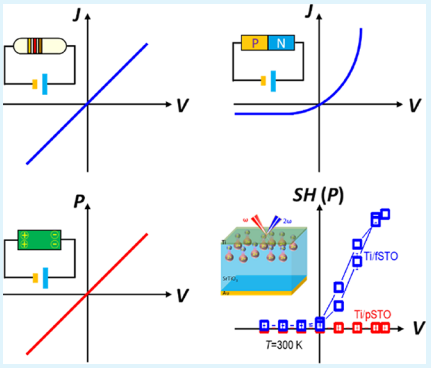

KEYWORDS: *polar rectification, pre-ferroelectric state, heterojunctions, Schottky junction, $SrTiO_3$*

1. INTRODUCTION

From the perspective of movability, charges can be divided into two types: itinerant and localized.[1] The movement of itinerant charge carriers generates a current under an electric field. Metal or ohmic-contacted heterojunctions exhibit symmetric $J-V$ curves where the intensity of current J is independent of the direction of electrical field V (Figure 1a). For heterojunctions with a non-ohmic contact, a rectifying effect with asymmetric $J-V$ relation is expected,[2] as schematically shown in Figure 1b. The rectification of itinerant charge carriers has become a key signal-processing tool in current electronics, ranging from power supplies to high-frequency detectors, smart phones, computers, TV sets, and wireless communications. The localized charges, on the other hand, can generate electric polarization when placed in an electric field. In general, the relationship between the polarization strength (P) and V is symmetric for either a single dielectric material or a non-ohmic-contacted heterointerface (Figure 1c). Finding an asymmetric $P-V$ characteristic (Figure 1d), i.e., polar rectification, is a natural expectation, and it may have potential applications in the field of switchable rectifiers, energy storage, and computation.

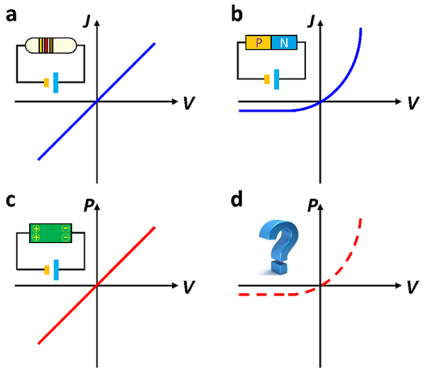

Figure 1. Schematic images of $J-V$ and $P-V$ relationships for typical electronic devices. (a) $J-V$ relationship of a resistor. (b) $J-V$ relationship of a $p-n$ junction. (c) $P-V$ relationship of a dielectric material. (d) $P-V$ relationship of a polar rectifier device.

In this context, the manipulation of remnant polarization, especially at the surface/interface, is of great importance for the creation of polar rectification. Recently, it has been shown that polar switching of ferroelectric thin films is sensitive to the electric boundary conditions at the surface/interface, including space charge generated from band bending or charged states formed from defects/surface adsorbates.[3,4] The electronic asymmetry at the ferroelectric surface/interface, especially space charge accumulated near the metal−ferroelectric

Received: May 7, 2020
Accepted: June 18, 2020
Published: June 18, 2020

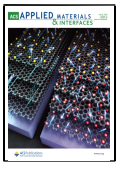

https://dx.doi.org/10.1021/acsami.0c08418
ACS Appl. Mater. Interfaces 2020, 12, 31645−31651

interfaces, can often generate displacement of the $P-V$ hysteresis loops, particularly along the electric field axis.[3,4] Such displacement is a biased effect with a negligible on/off ratio, and the polar rectification phenomenon has not been reported so far. However, the idea related to the localized charge manipulation near the metal−dielectric interfaces may provide a possible route for the realization of polar rectification.

Oxygen vacancies (OVs) in oxides can act as either mobile or localized donors, and their behavior at the metal−oxide interface can be controlled electrically.[5] As a typical transition-metal oxide with high dielectric constant, low dielectric loss, and good thermal stability, $SrTiO_3$ (STO) is widely used in inverter capacitors, resistance switching random access memories, and other electronic devices.[6,7] Considerable research efforts have been devoted to the OV-induced structural, electric, magnetic, and ferroelectric properties in STO single crystals and metal−STO heterojunctions.[6−13] In addition, STO was identified as an incipient ferroelectric material, which approaches but does not cross the ferroelectric phase transition due to quantum fluctuation.[14−16] Introducing OVs can suppress the quantum fluctuation and stabilize the ferroelectric phase of STO,[17] yet unidirectional electric polarization has not been reported.

Here, by repeatedly applying the electric field to a Ti/STO heterojunction, lots of OVs accumulate in the Ti/STO interface. Most of the oxygen vacancies are charged with 2+(Vo^{2+}), but there also exists neutral or 1+ because of the metastable Vo^{2+}.[18] Thus, an electro-fatigued STO (fSTO) crystal with OV−electron pairs is created. By controlling the movement of OV−electron pairs in the depletion layer of the Ti/fSTO junction, a polarization rectification effect is realized. Further structural, Raman, and nonlinear optical measurements show that such fSTO resides in the crossover regime between the pristine quantum paraelectric state and the ferroelectric state. A small external electric field (<1.2 kV/cm) can drive this pre-ferroelectric STO crystal into the ferroelectric phase within the temperature range from 50 to 170 K.

2. EXPERIMENTAL SECTION

2.1. Sample Fabrication. The Ti/STO/Au sandwiched samples for SH and dielectric measurements were obtained by depositing a 6 nm-thick Ti layer on the top and 100 nm-thick Au layer on the back side of a (001) STO substrate (3 × 5 × 0.5 mm^3, doubly polished). Ti (anode) was grown by magnetron sputtering in an Ar atmosphere of pressure 5 × 10^{-3} mbar at room temperature. Also, the Au layer (cathode) was grown through thermal evaporation in the vacuum chamber. Since the Ti layer is only 6 nm in thickness, the laser light can pass through it without obvious reflection from the metal layer. For the electro-fatigue process, the E_{ext} up to 10 kV/cm was applied on STO with a Keithley 2410 source. The 10 kV/cm field was maintained on Ti/STO for 30 min and then dropped down to zero. With sweeping up and down of E_{ext} for more than 10 times, more and more OVs are created and an electro-fatigued STO was produced. The detailed fatigue process and the monitoring data by second harmonic generation (SHG) can be found in Figure S1.

2.2. SHG Measurement. The 45° reflection geometry with a fundamental wavelength at 800 nm (150 fs duration at a 1 kHz repetition rate) was used here. A half-wave plate was used to rotate the polarization angle of the incident pump pulses, and a Glan prism was used to rotate the polarization angle of the output SH pulses. The SH photons, selected using a monochrometer, were transformed using a photomultiplier tube and then recorded using a lock-in amplifier (details can be found in Figure S2).

3. RESULTS AND DISCUSSION

The structure of the Ti/STO heterojunctions is sketched in Figure 2a. A (001)-orientated STO single crystal (5 × 5 × 0.5 mm^3) was covered by a 6 nm-thick Ti layer (anode) on the surface and a 100 nm-thick Au layer (cathode) on the back. Both pristine STO (pSTO) and fSTO samples were studied, with the latter produced by sweeping an electric field from 0 to 10 kV/cm up and down more than 10 times on the Ti/STO junction (Figure S1).[10,11] Before, during, and after the fatigue process, the electric polarization in the Ti/fSTO junction is measured by the SHG technique, which is highly sensitive to symmetry breaking and often used in probing electric polarization in ferroelectric crystals and thin films (Figure S2).[19−21] Figure 2b shows the SH intensity as a function of external electric field (E_{ext}) for both Ti/pSTO and Ti/fSTO heterojunctions. As sweeping E_{ext} from negative to positive values, the SH output signal for the Ti/pSTO junction is negligible and remains constant in the whole measured field range (red curve in Figure 2b). In contrast, for the Ti/fSTO case, it is apparent to find an asymmetric SH−E_{ext} loop as E_{ext} sweeps (blue curve in Figure 2b). When a negative E_{ext} is applied, i.e., Ti(−)/STO(+), the SH output signal is small and remains constant, similar to that of the pristine case. For positive E_{ext}, on the other hand, the SH intensity increases monotonously with increasing E_{ext}. The ratio of the SH signal for E_{ext} = +6 and −6 kV/cm is around 32, which can serve as the on/off ratio of this polar rectification junction. Apparently, in addition to the current rectifier devices based on itinerant charge, a polar rectifier device based on localized charges has been realized here.

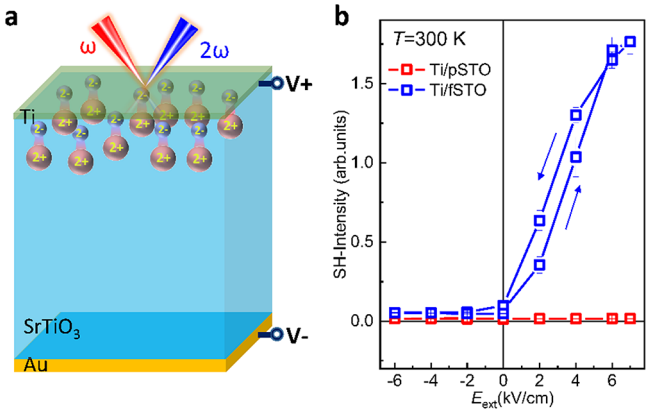

Figure 2. (a) Schematic image for a Ti/fSTO/Au heterojunction and SHG measurements for the electric polarization. The red and blue balls represent the oxygen vacancies and electrons, respectively. (b) Electric field-dependent SH intensity for both Ti/pSTO and Ti/fSTO junctions measured at T = 300 K. The arrows represent the electric field sweeping direction.

Comparing the SH−E_{ext} results of both pristine and electro-fatigued STO junctions, we conclude that the fatigue process of the STO crystal plays a key role in realizing polar rectification. As mentioned above, the fatigue process of the STO crystal was done by sweeping large E_{ext} up and down repeatedly in the Ti/STO junction. This is similar to the processes adopted in previous works,[10,11,22] where electric-field-fatigued STO was reported. During this fatigue process, it was also found that the Ti/STO interface can act as an oxygen getter.[10,11] The work function (Φ_M) of Ti is 4.33 eV. The band

https://dx.doi.org/10.1021/acsami.0c08418
ACS Appl. Mater. Interfaces 2020, 12, 31645−31651

gap, electron affinity, and charge neutrality level for $SrTiO_3$ are 3.3, 3.9, and 4.6 eV, respectively.[23−25] The bands line up between the work function of the metal and the charge neutrality level of STO, which gives a Schottky barrier height (built-in potential) of −0.27 eV (band bending down) for Ti/STO (Figure S3). The electric field in the interface of the depletion layer (E_{in}) is calculated at ∼40.2 kV/cm based on the sharp Schottky diode model (Figure S3), which is much larger than the E_{ext} applied here. When the applied E_{ext} is opposite to E_{in}, i.e., Ti(−)/STO(+), no OVs can be generated as E_{ext} is much smaller than E_{in}. For the Ti(+)/STO(−) case, however, the OVs can be continually generated near the Ti/STO interface when E_{ext} exceeds a critical value (E_c).[11] For the Ti/pSTO(001) junction, the E_c is around 8 kV/cm. In this work, with sweeping E_{ext} up and down between 0 and 10 kV/cm (>E_c), OVs are generated and migrate into the STO. After 10 electric cycles, many remnant OVs were produced near the Ti/STO interface and thus an electro-fatigued STO layer is created (Figure 2a). Due to the large intensity of E_{in}, most remnant OVs were located in the depletion layer of the Ti/STO junction. It was calculated that the width of depletion layer (W_d) increases from 100 nm to several micrometers when E_{ext} was swept from 0 to 10 kV/cm (Figure S3). We emphasize that such an electro-fatigue process can only be realized in the metal/STO junction with the bending down of the electron energy band. For the band bending up (Φ_M > 4.6 eV) cases, such as Au/STO, the remnant OVs and thus fSTO could not be produced due to the opposite direction of E_{in}, which has been confirmed by X-ray measurements (Figure S4). These features are also consistent with previous reports, in which the oxygen atoms were proved to be able to transfer from the STO to the metal layer, resulting in the formation of OVs in STO.[12,13,26]

To further confirm the existence of OVs in the fSTO, X-ray photoelectron spectroscopy (XPS) was performed. Figure 3a,b shows the high-resolution XPS spectra of Ti 2p and Sr 3d for the fatigued and pristine STO, respectively. These XPS data were calibrated by the C 1s spectra (Figure S5). Comparing with the pSTO, the XPS peaks of the fSTO shift to higher energy. Specifically, the peaks of Ti $2p_{1/2}$ and Ti $2p_{3/2}$ shift about 0.28 eV and the two peaks of Sr 3d shift about 0.25 eV. This indicates the existence of OVs in the STO.[27] In addition, X-ray diffraction (XRD) results show that the (002) diffraction peak of the fSTO crystal shifts to a lower 2θ angle (the inset of Figure 3a), which indicates the elongation of the c-axis and therefore the existence of OVs in the whole near-surface region.[10,11] Moreover, when the applied electric field is large enough, it can also cause another transient electrostrictive distortion effect (Figure S3).[28,29] There are two points worth of special attention. First, the critical electric field for the electro-induced crystal distortion of Ti/fSTO is larger than 12 kV/cm. In order to eliminate the contribution from the additional electrostrictive distortion effect, all the polar rectification measurements were done with the electric fields less than 6 kV/cm. Second, the observed electro-fatigue effect in STO has crystal axis orientation dependence. It was found that the E_{ext} = 10 kV/cm is enough for the fatigued (001)-oriented STO crystal, while it is insufficient for the (110) and (111) STOs (E_c > 10 kV/cm), which indicates that the creation and migration of OVs are harder in the latter two crystalline directions (Figure S1).

In fSTO, the ejection of the neutral oxygen leaves a lattice deformation (OV) and two extra electrons. These electrons

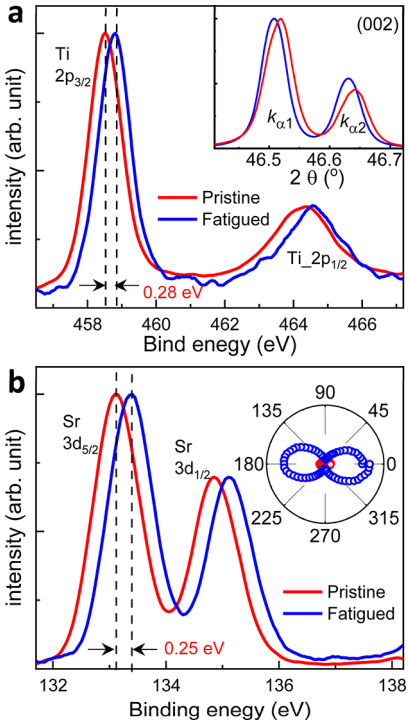

Figure 3. XPS spectra for both pSTO and fSTO crystals. (a) XPS spectra of Ti in STO crystals. The inset of (a) is the XRD results of the (002) peak for both pSTO and fSTO crystals. (b) XPS spectra of Sr in STO crystals. The inset of (b) is the polar plots of the SH intensity versus the polarization angle of output light for E_{ext} = 0 V/cm of pSTO and E_{ext} = 0 V/cm and 10 kV/cm of fSTO.

can stay in the OVs accompanied by strong relaxation of the neighborhood lattice (a polaron).[30] For simplicity, the OVs with attracted electrons are labeled as OV−electron charge pairs here. With an E_{ext} applied, the displacement of electrons from the OVs in the fSTO would produce an electric polarization, which contributed to the third-order susceptibilities χ_{ijkz} as well as the SHG. The effective SHG susceptibility for this case can be written as $\chi^{eff} = \chi_{ijkz}E_{ext}L$, in which L is the effective modulation depth of E_{ext}.[31−33] This provides us an efficient route to monitor the polarization state in the Ti/fSTO junction as used here.

The above analysis confirmed the existence of OV−electron charge pairs near the Ti/fSTO interface. Next, let us examine the E_{ext}-induced behavior of OV−electron charge pairs and the mechanism for emergent polar rectification, as shown in Figure 2b. When a conventional dielectric material, such as pSTO, is placed in an electric field, the positive and negative charges slightly shift from their average equilibrium positions in an opposite way. Nevertheless, the overall positive and negative charge centers in the material are still coincident. Then, there is no remnant electric polarization that exist, except minor field-induced charges on the surface, which would contribute to the polarization as well as a small SH output. The amount and the direction of those surficial charges are determined by both the intensity and the direction of E_{ext}. Hence, a symmetric P−E_{ext} relationship can be obtained (Figure 1c). This is the case for the Ti/pSTO junction (red curve in Figure 2b). However, the situation is different if there are excess charges, such as OVs. These excess OVs−electron pairs can be separated by E_{ext}, producing electric polarization as well as SH output, which has been confirmed by our experiments

https://dx.doi.org/10.1021/acsami.0c08418
ACS Appl. Mater. Interfaces 2020, 12, 31645−31651

(blue curve in Figure 2b). It should be noted that the movabilities of positive OVs and negative electrons are completely different. While the electrons can be easily moved by the electric field, as a structural defect, the movement of OVs requires higher energy, as proved by the fatigue process. The E_{ext} values in our study are smaller than the highest electric field used for the fatigue process (10 kV/cm), which only drives the electrons around essentially static OVs.

Figure 4a–c shows the schematic band diagram of Ti/fSTO Schottky junctions with different E_{ext} values. When E_{ext} = 0, the

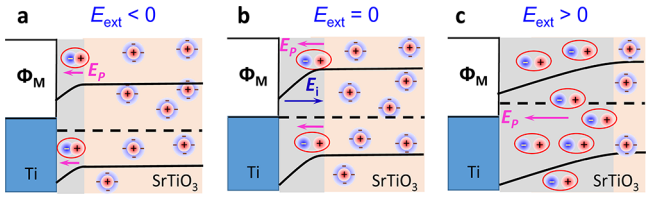

Figure 4. Schematic illustration of the energy band diagram of Ti/fSTO junctions. (a–c) Band structures with (a) E_{ext} < 0 V/cm, (b) E_{ext} = 0 V/cm, and (c) E_{ext} > 0 V/cm. The work function (Φ_M) of Ti is 4.33 eV, and the charge neutrality level of STO is 4.6 eV. The pink and blue arrows indicate the polarization direction of OV and electron pairs and the electric field in the depletion layer of the junction (E_i denotes the built-in electric field in the depletion layer; E_p denotes the polar direction of oxygen–electron pairs).

band bending and the charge accumulation happens in the W_d (~133.8 nm), accompanied with E_{in} pointing from Ti to STO (Figure 4b). The OV–electron pairs in the depletion layer were separated due to the existence of E_{in}, which produce a small remnant polarization as well as weak SH signals (Figure 2d and blue circles in the inset of Figure 3b). By comparing with the polarization of the $BaTiO_3$ film, this remnant polarization of Ti/fSTO is identified as 0.03 $\mu C/cm^2$. When E_{ext} < 0, W_d shrinks and the amount of OVs in the depletion layer is reduced. As a result, less polarization as well as weaker SH signals can be detected (Figure 2b). When E_{ext} > 0, as shown in Figure 4c, W_d extends wider and the number of OV–electron pairs in the depletion layer increases more. At the same time, the E_{ext}-induced separation of OV–electron pairs gives rise to much larger polarization and SH signals. It was found that, comparing to the SH result obtained with E_{ext} = 0, a 7 kV/cm E_{ext} causes a 25 times increase in SH output (Figure 2b and the inset of Figure 3b), which corresponds to a 5-fold enhancement of P. Obviously, due to the low movability of OVs and the variation of W_d in the Ti/fSTO Schottky junction, an asymmetric SH–E_{ext} relationship was obtained, as shown in the Figure 2b. Analogous to the current rectification in semiconductor heterojunctions, the polar rectification observed from the Ti/fSTO junction may have potential applications in memory devices, high voltage protection, and so on.

After examining polar rectification of the Ti/fSTO junction, let us get a chance to explore the fSTO crystal itself. As shown in the inset of Figure 3a, the OVs distort the lattice structure of the fSTO crystal, which may also give rise to a transition of the electronic phases of the STO crystal. To further clarify the exact phase state of fSTO, Raman spectra were measured at different temperatures and the typical results are shown in Figure 5. For pSTO, there is a cubic-to-antiferrodistortive (AFD) structure transition at $T_a \approx 105$ K and the E_g+B_{1g} (143

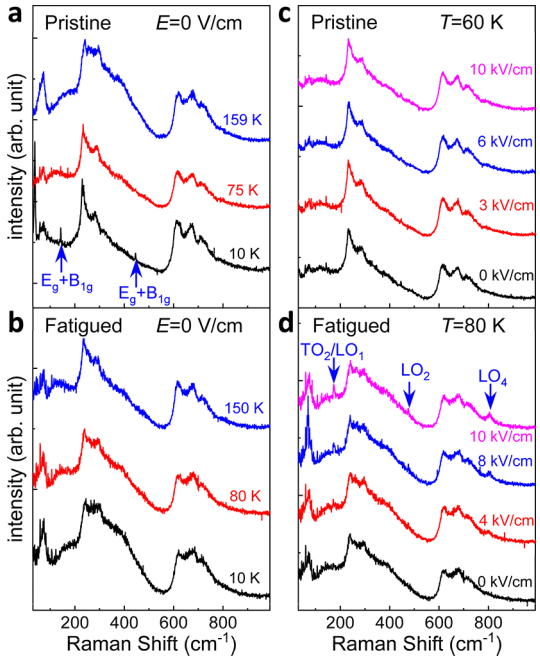

Figure 5. Raman spectra of pristine and fatigued STO. (a, b) Raman spectra at different temperatures when E = 0 V/cm for pristine STO and fatigued STO, respectively. (c, d) Raman spectra at different electric fields of pristine STO (T = 80 K) and fatigued STO (T = 60 K), respectively. The blue arrows in (a) indicate the E_{1g}+B_{1g} modes. The blue arrows in (d) indicate the TO/LO modes.

and 446 cm^{-1}) Raman modes emerge below T_a.[34] This has been confirmed by Figure 5a. For fSTO, however, the Raman spectra are almost temperature-independent (Figure 5b). No E_g+B_{1g} Raman modes are found below 10 K, which implies the suppression of the AFD structure transition by OVs. More than that, no ferroelectric phase is formed, as implied by the absence of first-order LO phonon modes that has been identified as the signature of a ferroelectric phase in perovskite oxides.[35] Figure 5c,d shows the Raman spectra under E_{ext} for both pristine and fatigued STO measured at T = 60 and 80 K, respectively. It was found that the Raman spectra of pSTO are insensitive to the electric field up to 10 kV/cm. Interestingly, a series of first-order LO phonon Raman modes, i.e., peaks at 173 cm^{-1} (LO1/TO2), 475 cm^{-1} (LO3), and 803 cm^{-1} (LO4), as well as the ferroelectric structural phase were induced in fSTO by the external electric field.[35] It implies that, comparing with pSTO, the fSTO can be easily driven into the ferroelectric state. These observations indicate that the OVs in fSTO have suppressed AFD and driven the STO to the border of the FE phase. From this viewpoint, it is reasonable to deduce that the fSTO is in a pre-ferroelectric state.

To further explore the pre-ferroelectric state in fSTO, the temperature-dependent SH output has been studied. As depicted in Figure 6, the SH measurement of pSTO shows that there is almost no spontaneous polarization in the whole measurement temperature range. As for the fatigued sample, there is an upturn of SH signals around 170 K and a drop of SH output below 40 K (red curve in Figure 6). This feature implies that there are three sub-states for the pre-ferroelectric STO crystal at different temperatures. We assign them as pre-ferroelectric state I (T > 170 K), II (40–170 K), and III (below 40 K). To further study the different pre-ferroelectric states of fatigued STO, the temperature-dependent SH

https://dx.doi.org/10.1021/acsami.0c08418
ACS Appl. Mater. Interfaces 2020, 12, 31645–31651

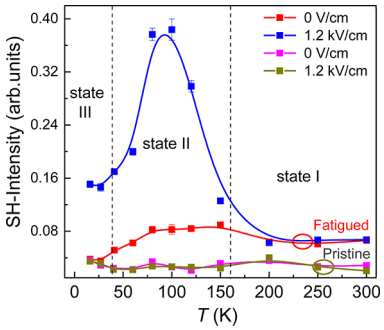

Figure 6. Temperature dependence of SH intensity for fatigued and pristine STO with E_{ext} = 0 and 1.2 kV/cm, respectively.

measurements with application of a small electric field (E_{ext} = 1.2 kV/cm) were done (blue curve in Figure 6). For pre-ferroelectric state I, there is a negligible effect on the SH signal with such small E_{ext}. When the fSTO get into pre-ferroelectric state II, a large enhancement of SH output was found. Around 80 K, the SH is enlarged more than five times by a 1.2 kV/cm electric field. Such electric field enhancement remains below 40 K, which implies that the application of E_{ext} helps suppress quantum fluctuation in the fSTO. However, as shown in Figure 6, the polarization gets a large reduction from pre-ferroelectric state II to III even with a bias field. This indicates that there is a competition between the quantum fluctuation and external electric field, and the electric field applied here can only partially suppress the quantum fluctuation. The temperature dependence of the pre-ferroelectric state might originate from the temperature dependence of ionization of OVs in fSTO. Based on the SH results, it seems that the OV−electron pairs are more easily separated in a temperature range of 40−170 K, which may be attributed to the structural transition of the fSTO crystal within this temperature range.

4. CONCLUSIONS

In conclusion, by utilizing the electric field sweeping technique, the fSTO with OVs inside was created. Taking advantages of different movabilities between OVs and electrons in the depletion layer, a polar rectification was realized for the first time in a Ti/fSTO heterojunction. The temperature and electric field varied SH output and X-ray diffraction and Raman measurements, and we identified that such STO owns a pre-ferroelectric state, which is just between quantum paraelectric and ferroelectric states. Moreover, it is interesting to find that the fSTO with a pre-ferroelectric state is easily driven into a ferroelectric state by an external electric field. These findings not only give a further path to study the ferroelectric state of perovskite oxides but also provide a novel electric rectification device that may be a building block in future electronics.

■ ASSOCIATED CONTENT

Supporting Information

The Supporting Information is available free of charge at https://pubs.acs.org/doi/10.1021/acsami.0c08418.

Electrodegradation process for the fatigued $SrTiO_3$, second harmonic generation (SHG) measurements, band structural analysis of the Ti/$SrTiO_3$/Au junctions, XRD results for both Ti/$SrTiO_3$ and Au/$SrTiO_3$ junctions with application of E_{ext}, and calibration of X-ray photoelectron spectroscopy (XPS) spectra (PDF).

■ AUTHOR INFORMATION

Corresponding Authors

Zhigao Sheng − *Anhui Province Key Laboratory of Condensed Matter Physics at Extreme Conditions, High Magnetic Field Laboratory, Chinese Academy of Science, Hefei 230031, China; Key Laboratory of Photovoltaic and Energy Conservation Materials, Institute of Applied Technology, Chinese Academy of Sciences, Hefei 230031, China;* orcid.org/0000-0003-3382-5968; Email: zhigaosheng@hmfl.ac.cn

Jirong Sun − *Beijing National Laboratory for Condensed Matter Physics, Institute of Physics, Chinese Academy of Sciences, Beijing 100190, China;* orcid.org/0000-0003-1238-8770; Email: jrsun@iphy.ac.cn

Zhicheng Zhong − *Key Laboratory of Magnetic Materials and Devices, Zhejiang Province Key Laboratory of Magnetic Materials and Application Technology, Ningbo Institute of Materials Technology and Engineering, Chinese Academy of Sciences, Ningbo 315201, China;* orcid.org/0000-0003-1507-4814; Email: zhong@nimte.ac.cn

Authors

Xueli Xu − *Anhui Province Key Laboratory of Condensed Matter Physics at Extreme Conditions, High Magnetic Field Laboratory, Chinese Academy of Science, Hefei 230031, China; University of Science and Technology of China, Hefei, Anhui 230026, China; Key Laboratory of Photovoltaic and Energy Conservation Materials, Institute of Applied Technology, Chinese Academy of Sciences, Hefei 230031, China*

Hui Zhang − *Fert Beijing Institute, School of Microelectronics, Beijing Advanced Innovation Center for Big Data and Brain Computing, Beihang University, Beijing 100191, China; Beijing National Laboratory for Condensed Matter Physics, Institute of Physics, Chinese Academy of Sciences, Beijing 100190, China*

Ranran Zhang − *Anhui Province Key Laboratory of Condensed Matter Physics at Extreme Conditions, High Magnetic Field Laboratory, Chinese Academy of Science, Hefei 230031, China*

Lihua Yin − *Key Laboratory of Materials Physics, Institute of Solid State Physics, Chinese Academy of Sciences, Hefei 230031, China;* orcid.org/0000-0002-6993-1140

Yuping Sun − *Key Laboratory of Materials Physics, Institute of Solid State Physics, Chinese Academy of Sciences, Hefei 230031, China*

Haoliang Huang − *Anhui Laboratory of Advanced Photon Science and Technology, National Synchrotron Radiation Laboratory, University of Science and Technology of China, Hefei 230026, P. R. China;* orcid.org/0000-0002-5686-5519

Yalin Lu − *Anhui Laboratory of Advanced Photon Science and Technology, National Synchrotron Radiation Laboratory, University of Science and Technology of China, Hefei 230026, P. R. China*

Yi Lu − *Institute for Theoretical Physics, Heidelberg University, 69120 Heidelberg, Germany*

Chun Zhou − *Anhui Province Key Laboratory of Condensed Matter Physics at Extreme Conditions, High Magnetic Field Laboratory, Chinese Academy of Science, Hefei 230031, China*

Zongwei Ma − *Anhui Province Key Laboratory of Condensed Matter Physics at Extreme Conditions, High Magnetic Field Laboratory, Chinese Academy of Science, Hefei 230031, China;* orcid.org/0000-0002-9328-9194

Lei Shen − *Anhui Province Key Laboratory of Condensed Matter Physics at Extreme Conditions, High Magnetic Field Laboratory, Chinese Academy of Science, Hefei 230031, China;*

https://dx.doi.org/10.1021/acsami.0c08418
ACS Appl. Mater. Interfaces 2020, 12, 31645−31651

University of Science and Technology of China, Hefei, Anhui 230026, China

Junsong Wang − *Anhui Province Key Laboratory of Condensed Matter Physics at Extreme Conditions, High Magnetic Field Laboratory, Chinese Academy of Science, Hefei 230031, China*

Jiandong Guo − *Beijing National Laboratory for Condensed Matter Physics, Institute of Physics, Chinese Academy of Sciences, Beijing 100190, China;* orcid.org/0000-0002-7893-022X

Complete contact information is available at: https://pubs.acs.org/10.1021/acsami.0c08418

Author Contributions

◆X.X. and H.Z. contributed equally to this work.

Notes

The authors declare no competing financial interest.

■ ACKNOWLEDGMENTS

This work is supported by the National Key R&D Program of China (grant nos. 2017YFA0303603, 2018YFA0305704, and 2016YFA0401803), the National Natural Science Foundation of China (NSFC; grant nos. 11574316, 11934016, 11520101002, and U1532155), the Key Research Program of Frontier Sciences, CAS (grant no. QYZDB-SSW-SLH011), the Innovative Program of Development Foundation of Hefei Center for Physical Science and Technology (grant no. 2016FXCX002), and the One Thousand Youth Talents Program of China. A portion of this work was performed on the Steady High Magnetic Field Facilities (ultrafast optical measurement system under superconducting magnet), High Magnetic Field Laboratory, CAS, and supported by the Anhui Laboratory of High Magnetic Field.

■ REFERENCES

(1) Kittel, C.; McEuen, P. *Introduction to Solid State Physics*; FifthEd., Wiley: United Kingdom, 1976.

(2) Sze, S. M.; Ng, K. K. *Physics of Semiconductor Devices*; Wiley, 2006.

(3) Yang, M.; Amit, K. C.; Garcia-Castro, A. C.; Borisov, P.; Bousquet, E.; Lederman, D.; Romero, A. H.; Cen, C. Room Temperature Ferroelectricity in Fluoroperovskite Thin Films. *Sci. Rep.* **2017**, *7*, 7182.

(4) Misirlioglu, I. B.; Okatan, M. B.; Alpay, S. P. Asymmetric Hysteresis Loops and Smearing of the Dielectric Anomaly at the Transition Temperature Due to Space Charges in Ferroelectric Thin Films. *J. Appl. Phys.* **2010**, *108*, No. 034105.

(5) Jiang, W.; Noman, M.; Lu, Y. M.; Bain, J. A.; Salvador, P. A.; Skowronski, M. Mobility of Oxygen Vacancy in $SrTiO_3$ and its Implications for Oxygen-Migration-Based Resistance Switching. *J. Appl. Phys.* **2011**, *110*, No. 034509.

(6) Cai, H. L.; Wu, X. S.; Gao, J. Effect of Oxygen Content on Structural and Transport Properties in $SrTiO_{3-x}$ Thin Films. *Chem. Phys. Lett.* **2009**, *467*, 313−317.

(7) Trabelsi, H.; Bejar, M.; Dhahri, E.; Sajieddine, M.; Khirouni, K.; Prezas, P. R.; Melo, B. M. G.; Valente, M. A.; Graça, M. P. F. Effect of Oxygen Vacancies on $SrTiO_3$ Electrical Properties. *J. Alloys Compd.* **2017**, *723*, 894−903.

(8) Wang, C. C.; Lei, C. M.; Wang, G. J.; Sun, X. H.; Li, T.; Huang, S. G.; Wang, H.; Li, Y. D. Oxygen-Vacancy-Related Dielectric Relaxations in $SrTiO_3$ at High Temperatures. *J. Appl. Phys.* **2013**, *113*, No. 094103.

(9) Brovko, O. O.; Tosatti, E. Controlling the Magnetism of Oxygen Surface Vacancies in $SrTiO_3$ through Charging. *Phys. Rev. Mater.* **2017**, *1*, No. 044405.

(10) Li, Y.; Lei, Y.; Shen, B. G.; Sun, J. R. Visible-Light-Accelerated Oxygen Vacancy Migration in Strontium Titanate. *Sci. Rep.* **2015**, *5*, 14576.

(11) Hanzig, J.; Zschornak, M.; Hanzig, F.; Mehner, E.; Stöcker, H.; Abendroth, B.; Röder, C.; Talkenberger, A.; Schreiber, G.; Rafaja, D.; Gemming, S.; Meyer, D. C. Migration-Induced Field-Stabilized Polar Phase in Strontium Titanate Single Crystals at Room Temperature. *Phys. Rev. B* **2013**, *88*, No. 024104.

(12) Li, Y.; Wang, Q.; An, M.; Li, K.; Wehbe, N.; Zhang, Q.; Dong, S.; Wu, T. Nanoscale Chemical and Valence Evolution at the Metal/Oxide Interface: A Case Study of $Ti/SrTiO_3$. *Adv. Mater. Interfaces* **2016**, *3*, 1600201.

(13) Fu, Q.; Wagner, T. Interaction of Nanostructured Metal Overlayers with Oxide Surfaces. *Surf. Sci. Rep.* **2007**, *62*, 431−498.

(14) Unoki, H.; Sakudo, T. Electron Spin Resonance of Fe^{3+} in $SrTiO_3$ with Special Reference to 110°K Phase Transition. *J. Phys. Soc. Jpn.* **1967**, *23*, 546−552.

(15) Zhong, W.; Vanderbilt, D. Competing Structural Instabilities in Cubic Perovskites. *Phys. Rev. Lett.* **1995**, *74*, 2587−2590.

(16) Singh, S.; Sangle, A. L.; Wu, T.; Khare, N.; MacManus-Driscoll, J. L. Growth of Doped $SrTiO_3$ Ferroelectric Nanoporous Thin Films and Tuning of Photoelectrochemical Properties with Switchable Ferroelectric Polarization. *ACS Appl. Mater. Interfaces* **2019**, *11*, 45683−45691.

(17) Bussmannholder, A.; Bilz, H.; Bäuerle, D.; Wagner, D. A Polarizability Model for the Ferroelectric Mode in Semiconducting $SrTiO_3$. *Z. Phys. B Condens. Matter* **1981**, *41*, 353−355.

(18) Hu, W. J.; Paudel, T. R.; Lopatin, S.; Wang, Z.; Ma, H.; Wu, K.; Bera, A.; Yuan, G.; Gruverman, A.; Tsymbal, E. Y.; Wu, T. Colossal X-Ray-Induced Persistent Photoconductivity in Current-Perpendicular-to-Plane Ferroelectric/Semiconductor Junctions. *Adv. Funct. Mater.* **2017**, *28*, 1704337.

(19) Bloembergen, N.; Pershan, P. S. Light Waves at Boundary of Nonlinear Media. *Phys. Rev.* **1962**, *128*, 606−622.

(20) Shen, Y. R. Optical Second Harmonic-Generation at Interfaces. *Annu. Rev. Phys. Chem.* **1989**, *40*, 327−350.

(21) Fiebig, M.; Pavlov, V. V.; Pisarev, R. V. Second-Harmonic Generation as A Tool for Studying Electronic and Magnetic Structures of Crystals: Review. *J. Opt. Soc. Am. B* **2005**, *22*, 96−118.

(22) Jalan, B.; Engel-Herbert, R.; Mates, T. E.; Stemmer, S. Effects of Hydrogen Anneals on Oxygen Deficient $SrTiO_{3-x}$ Single Crystals. *Appl. Phys. Lett.* **2008**, *93*, No. 052907.

(23) Hikita, Y.; Kozuka, Y.; Susaki, T.; Takagi, H.; Hwang, H. Y. Characterization of the Schottky Barrier in $SrRuO_3$/Nb : $SrTiO_3$ Junctions. *Appl. Phys. Lett.* **2007**, *90*, 143507.

(24) Robertson, J.; Chen, C. W. Schottky Barrier Heights of Tantalum Oxide, Barium Strontium Titanate, Lead Titanate, and Strontium Bismuth Tantalate. *Appl. Phys. Lett.* **1999**, *74*, 1168−1170.

(25) Zhong, Z.; Hansmann, P. Tuning the Work Function in Transition Metal Oxides and Their Heterostructures. *Phys. Rev. B* **2016**, *93*, 235116.

(26) Trier, F. *Quantum and Field Effects of Oxide Heterostructures*; Department of Energy Conversion and Storage, Technical University of Denmark, 2016.

(27) Tan, H.; Zhao, Z.; Zhu, W.-b.; Coker, E. N.; Li, B.; Zheng, M.; Yu, W.; Fan, H.; Sun, Z. Oxygen Vacancy Enhanced Photocatalytic Activity of Pervoskite $SrTiO_3$. *ACS Appl. Mater. Interfaces* **2014**, *6*, 19184−19190.

(28) Ascienzo, D.; Kurt, O.; Greenbaum, S.; Bayer, T. J. M.; Maier, R. A.; Randall, C. A.; Ren, Y. Formation of Structural Defects and Strain in Electrodegraded Fe-Doped $SrTiO_3$ Crystals Due to Oxygen Vacancy Migration. *J. Am. Ceram. Soc.* **2018**, *101*, 2545−2561.

(29) Ascienzo, D.; Kurt, O.; Greenbaum, S.; Bayer, T. J. M.; Russell, M.; Wang, J.; Randall, C. A.; Ren, Y. Local Structural Changes Due to the Electric Field-Induced Migration of Oxygen Vacancies at Fe-doped $SrTiO_3$ Interfaces. *J. Am. Ceram. Soc.* **2019**, *102*, 4353−4366.

(30) Jackmana, M. J.; Deák, P.; Syres, K. L.; Adell, J.; Thiagarajan, B.; Levy, A.; Thomas, A. G. Observation of Vacancy-Related Polaron

States at the Surface of Anatase and Rutile TiO_2 by Highresolution Photoelectron Spectroscopy. *arXiv.* **2014**, *1406*, 3385.
(31) Terhune, R. W.; Maker, P. D.; Savage, C. M. Optical Harmonic Generation in Calcite. *Phys. Rev. Lett.* **1962**, *8*, 404−406.
(32) Klein, J.; Wierzbowski, J.; Steinhoff, A.; Florian, M.; Rösner, M.; Heimbach, F.; Müller, K.; Jahnke, F.; Wehling, T. O.; Finley, J. J.; Kaniber, M. Electric-Field Switchable Second-Harmonic Generation in Bilayer MoS_2 by Inversion Symmetry Breaking. *Nano Lett.* **2017**, *17*, 392−398.
(33) Chen, S.; Li, K. F.; Li, G.; Cheah, K. W.; Zhang, S. Gigantic Electric-Field-Induced Second Harmonic Generation from an Organic Conjugated Polymer Enhanced by A Band-Edge Effect. *Light: Sci. Appl.* **2019**, *8*, 17.
(34) Petzelt, J.; Ostapchuk, T.; Gregora, I.; Rychetský, I.; Hoffmann-Eifert, S.; Pronin, A. V.; Yuzyuk, Y.; Gorshunov, B. P.; Kamba, S.; Bovtun, V.; Pokorný, J.; Savinov, M.; Porokhonskyy, V.; Rafaja, D.; Vaněk, P.; Almeida, A.; Chaves, M. R.; Volkov, A. A.; Dressel, M.; Waser, R. Dielectric, Infrared, And Raman Response of Undoped $SrTiO_3$ Ceramics: Evidence of Polar Grain Boundaries. *Phys. Rev. B* **2001**, *64*, 184111.
(35) Jang, H. W.; Kumar, A.; Denev, S.; Biegalski, M. D.; Maksymovych, P.; Bark, C. W.; Nelson, C. T.; Folkman, C. M.; Baek, S. H.; Balke, N.; Brooks, C. M.; Tenne, D. A.; Schlom, D. G.; Chen, L. Q.; Pan, X. Q.; Kalinin, S. V.; Gopalan, V.; Eom, C. B. Ferroelectricity in Strain-Free $SrTiO_3$ Thin Films. *Phys. Rev. Lett.* **2010**, *104*, 197601.

https://dx.doi.org/10.1021/acsami.0c08418
ACS Appl. Mater. Interfaces 2020, 12, 31645−31651